

# Loss mechanisms in mid-infrared extraordinary optical transmission gratings

T. Ribaldo,<sup>1</sup> B. Passmore,<sup>2</sup> K. Freitas,<sup>1</sup> E.A. Shaner,<sup>2</sup> J.G. Cederberg,<sup>2</sup> and D. Wasserman<sup>1,\*</sup>

<sup>1</sup>Department of Physics and Applied Physics, University of Massachusetts Lowell, One University Avenue, Lowell, MA, 01854, USA

<sup>2</sup>Sandia National Labs, P.O. Box 5800, Albuquerque, NM 87185

\*Corresponding author: [daniel.wasserman@uml.edu](mailto:daniel.wasserman@uml.edu)

**Abstract:** The optical properties of periodic arrays of subwavelength apertures in metal films on GaAs substrates are studied. Specifically, geometric and material losses for these plasmonic structures are characterized using angular dependent transmission, normal incidence reflection, and angular dependent diffraction experiments, in addition to a crossed-polarizer transmission experiment. The optical properties of the samples as a function of engineered material losses are studied. Using this comprehensive approach to the characterization of the plasmonic structures, we are able to identify and isolate specific loss mechanisms, as well as identify the effect of free carriers on the optical properties of the structures.

©2008 Optical Society of America

**OCIS codes:** (050.2770) Gratings; (240.6680) Surface plasmons; (050.6624) Subwavelength structures

---

## References and links

1. D. L. Jeanmaire and R. P. Van Duyne, "Surface Raman Electrochemistry Part I. Heterocyclic, Aromatic and Aliphatic Amines Adsorbed on the Anodized Silver Electrode," *J. Electro. Anal. Chem.* **84** 1–20 (1977).
2. C. Genet and T. W. Ebbesen, "Light in Tiny Holes," *Nature* **445**, 39-46 (2007).
3. J. T. Kim, J. J. Ju, S. Park, M. Kim, S. K. Park, and M. Lee, "Chip-to-chip optical interconnect using gold long-range surface plasmon polariton waveguides," *Opt. Express* **16**, 13133-13138 (2008).
4. L. Martín-Moreno, F. J. García-Vidal, H. J. Lezec, A. Degiron, and T. W. Ebbesen, "Theory of Highly Directional Emission from a Single Subwavelength Aperture Surrounded by Surface Corrugations," *Phys. Rev. Lett.* **90**, 167401 (2003).
5. A. M. Gobin, M. H. Lee, N. J. Halas, W. D. James, R. A. Drezek, and J. L. West, "Near-Infrared Resonant Nanoshells for Combined Optical Imaging and Photothermal Cancer Therapy," *Nano. Lett.* **7**, 1929-1934 (2007).
6. T. W. Ebbesen, H. J. Lezec, H. F. Ghaemi, T. Thio, and P. A. Wolff, "Extraordinary optical transmission through sub-wavelength hole arrays," *Nature* **391**, 667-669 (1998).
7. H. A. Bethe, "Theory of diffraction by small holes," *Phys. Rev.* **66**, 163–182 (1944).
8. S. M. Williams, A. D. Stafford, K. R. Rodriguez, T. M. Rogers, and J. V. Coe, "Accessing Surface Plasmons with Ni Microarrays for Enhanced IR Absorption by Monolayers," *J. Phys. Chem. B* **107**, 11871-11879 (2003).
9. H. Liu and P. Lalanne, "Microscopic Theory of Extraordinary transmission," *Nature* **452**, 728-731 (2008).
10. D. Pacifici, H. J. Lezec, and H. A. Atwater, "Quantitative determination of optical transmission through subwavelength slit arrays in Ag films: Role of surface wave interference and local coupling between adjacent slits," *Phys. Rev. B* **77**, 115411 (2008).
11. D. Pacifici, H. J. Lezec, R. J. Walters, and H. A. Atwater, "Universal optical transmission features in periodic and quasiperiodic hole arrays," *Opt. Express* **16**, 9222-9238 (2008).
12. J. V. Coe, S. M. Williams, S. M. Teeters-Kennedy, K. R. Rodriguez, and S. Shah, "Scaffolding for Nanotechnology: Extraordinary IR Transmission of Metal Microarrays for Stacked Sensors and Surface Spectroscopy," *Nanotechnology* **15**, S495-S503 (2004).
13. A. Kastalsky, T. Duffield, S. J. Allen, and J. Harbison, "Photovoltaic detection of infrared light in a GaAs/AlGaAs superlattice," *Appl. Phys. Lett.* **52**, 1320-1322 (1988).
14. D. Pan and E. Towe, "Normal incidence intersubband (In,Ga)As/GaAs quantum dot infrared photodetectors," *Appl. Phys. Lett.* **73**, 1937-1939 (1998)

15. K. W. Berryman, S. A. Lyon, M. Segev, "Electronic structure and optical behavior of self-assembled InAs quantum dots," *J. Vac. Sci. Technol. B*, **15**, 1045-1050 (1997).
16. J. Faist, F. Capasso, D. L. Sivco, C. Sirtori, A. Hutchinson, and A. Cho, "Quantum cascade laser," *Science* **264**, 553-556 (1994).
17. N. Yu, J. Fan, Q. J. Wang, C. Pflügl, L. Diehl, T. Edamura, M. Yamanishi, H. Kan, and F. Capasso, "Small-divergence semiconductor lasers by plasmonic collimation," *Nature Photonics* **2**, 564-570 (2008).
18. D. Wasserman, and S. A. Lyon, "Midinfrared luminescence from InAs quantum dots in unipolar devices," *Appl. Phys. Lett.* **81**, 2848-2850 (2002).
19. A. V. Krasavin, A. V. Zayats, and N. I. Zheludev, "Active control of surface plasmon-polariton waves," *J. Opt. A: Pure Appl. Opt.* **7**, S8d-S89 (2005).
20. J. Y. Suh, E. U. Donev, R. Lopez, L. C. Feldman, and R. F. Haglund Jr., "Modulated optical transmission of subwavelength hole arrays in metal-VO<sub>2</sub> films," *Appl. Phys. Lett.* **88**, 133115 (2006).
21. E. A. Shaner, J. Cederberg, D. Wasserman, "Current-tunable mid-infrared extraordinary transmission gratings," *Appl. Phys. Lett.* **91**, 181110 (2007).
22. D. Wasserman, E. A. Shaner, and J. G. Cederberg, "Mid-Infrared doping tunable extraordinary transmission from sub-wavelength gratings," *Appl. Phys. Lett.* **90**, 191102 (2007).
23. M. Sarraazin, J. Vigneron, and J. Vigoureux, "Role of wood anomalies in optical properties of thin metallic films with a bidimensional array of subwavelength holes," *Phys. Rev. B*, **67** 085415 (2003).
24. T. J. Kim, T. Thio, T. W. Ebbesen, D. E. Grupp, and H. J. Lezec, "Control of optical transmission through metals perforated with subwavelength hole arrays," *Opt. Lett.* **24**, 256-258 (1999).
25. C. Billaudeau, S. Collin, C. Sauvan, N. Bardou, F. Pardo, and J. Pelouard, "Angle. Resolved transmission measurements through anisotropic two-dimensional Plasmonic crystals," *Opt. Lett.* **33**, 165-167 (2008).
26. R. W. Wood, *Proc. Phil. Mag.* **4**, 396-408 (1902).
27. L. Pang, K. A. Tetz, and Y. Fainman, "Observation of the splitting of degenerate surface plasmon polariton modes in a two-dimensional metallic nanohole array," *Appl. Phys. Lett.* **90**, 111103 (2007).
28. S. Chang, S. Gray, and G. Schatz "Surface plasmon generation and light transmission by isolated nanohole and arrays of nanoholes in thin metal films," *Opt. Express* **13**, 3150-3165 (2005).
29. H. F. Ghaemi, T. Thio, D. E. Grupp, T. W. Ebbesen, and H. J. Lezec, "Surface plasmons enhance optical transmission through subwavelength holes," *Phys. Rev. B* **58**, 6779-6782 (1998).

## 1. Introduction

There has been a growing interest in the optical properties of subwavelength metallic structures. By controlling the geometry of such structures, very strong and sharp optical resonances can be achieved, leading to improved materials for sensing [1], display [2], optical interconnects [3], beam steering [4] and medical applications [5]. In particular, periodic arrays of apertures in metallic films have been shown to enhance the transmission of light at wavelengths greater than an individual aperture's diameter [6]. This phenomenon, referred to as Extraordinary Optical Transmission (EOT), was first reported by Ebbesen, et al, and has been studied for its clear contradictions with conventional aperture theory [7], as well as for possible uses in applications such as chemical sensing [8] and display technologies [2].

It was initially argued that EOT is a result of light incident upon an aperture array coupling to, and subsequently reradiating out of, surface plasmon polariton (SPP) modes at the interface between the metal and the surrounding dielectric media. More recently, theoretical studies have reinforced the SPP as the dominant mechanism in EOT, but have also deepened the understanding of the phenomenon both by modeling the microscopic behavior of light at these interfaces and by studying the interplay between various surface waves and directly transmitted light on EOT gratings [9-11].

Much of the research in the field of EOT structures focuses on passive device schemes designed for use in the visible or near-IR wavelength ranges. However, the mid-infrared (mid-IR) wavelength range (3-20 $\mu$ m) offers significant opportunities for the development of plasmonic structures for sensing applications in the "fingerprint" regime of molecular absorption [12] and for the steering of mid-IR radiation. In addition, the mid-IR offers a vital test bed for plasmonic technologies at shorter wavelengths, as the longer wavelengths of the mid-IR frequencies result in corresponding increases in the scale, and therefore the ease of fabrication, of subwavelength structures.

An additional, powerful rationale for mid-IR plasmonic research is the potential development of hybrid electronic/plasmonic structures. In the mid-IR, semiconductors are transparent, while in much of the near-IR and visible wavelength ranges, propagation of SP's

at semiconductor/metal interfaces would not be possible due to interband absorption. Thus, SP-based structures might well prove valuable for enhancing the coupling of free space photons to and from mid-IR optoelectronic devices such as quantum well and quantum dot mid-IR photodetectors [13, 14] and emitters [15-18]. Even more enticing is the possibility of developing active plasmonic devices [19-21], where the SP resonance can be tuned by the application of an electrical signal.

The complex dielectric of an n-type semiconductor, using the Drude approximation, can be expressed as:

$$\varepsilon(\omega) = \varepsilon_s \left(1 - \frac{\omega_p^2}{\omega^2 + i\Gamma\omega}\right), \quad \omega_p^2 = \frac{n e^2}{\varepsilon_0 m^*}, \quad (1)$$

Where  $\omega_p$  is the plasma frequency,  $n$  is the carrier concentration,  $e$  is the charge of an electron,  $\varepsilon_s$  is the background dielectric constant of the semiconductor, and  $m^*$  is the effective electron mass in the semiconductor. Significant shifts in the dielectric function of a semiconductor can be realized by readily achievable shifts in the carrier concentration of the material. Because the SP resonance frequency depends, in part, on the dielectric constant of the dielectric material [9], the SP resonance can be tuned by controlling the carrier concentration at the semiconductor/metal interface. In fact, a significant shift in the spectral position of the SP resonance was recently demonstrated for EOT gratings fabricated upon GaAs epilayers doped with varying concentrations [22]. Since the basis of modern electronics involves the control of carrier concentration using an applied bias (the field effect transistor), these results show the feasibility of developing active, voltage controlled SP devices.

However, in order to effectively develop both enhanced mid-IR optoelectronic devices, and active plasmonic structures based on carrier concentration tuning, a thorough understanding of the loss mechanisms for semiconductor SP structures is required. Moreover, it would be unrealistic to presume that EOT is the only effect determining the optical properties of a periodically patterned metal/semiconductor interface. In fact, there are multiple effects contributing to the observed interaction of these gratings with incident light, as will be demonstrated in the following pages. Thus, this paper describes a thorough investigation into multiple loss mechanisms in semiconductor based plasmonic structures.

## 2. Experiment

In order to evaluate the loss mechanisms in EOT gratings, six samples were grown on semi-insulating GaAs epi-ready substrates. The total epitaxial growth thickness for each of the six samples was 1 $\mu$ m, but the epilayer structures for each sample differed in n-type (Si) doping concentrations and doped layer thickness, as shown in Table 1. Following growth, a standard photolithography, metal deposition, and lift-off process resulted in patterned metal layers (10/50nm Ti/Au) with a square, 3 $\mu$ m period array of 1.5  $\mu$ m diameter apertures, designed for peak transmission near a wavelength of 10  $\mu$ m.

Table 1. Epilayer growth structures of samples studied.

Sample	Doping Concentration (cm <sup>-3</sup> )	Doped Layer Thickness (nm)
A	0	NA
B	1E17	250
C	5E17	250
D	1E18	100
E	1E18	250
F	1E18	500

Because the dielectric constant of GaAs varies significantly in the Mid-IR wavelength range with free carrier concentrations, Eq. (1), identical EOT grating patterns on different samples will show a spectral shift in their resonant transmission peaks as a function of the carrier density and thickness of the doped layer. In addition, losses associated with free

carrier absorption can be simultaneously evaluated, by noting the percentage of transmitted light at the EOT resonant transmission spectral peak. Because the samples studied in this work cover a wide range of doping densities and doping thicknesses, we are able to determine the effect of carrier density and proximity to the metal/semiconductor surface on the optical properties of plasmonic structures. Doing so will allow for the optimization of both active and passive semiconductor/plasmonic structures.

A variety of experiments were utilized to characterize the samples studied in this work. For each experiment, a Bruker Vertex70 Fourier Transform Infrared (FTIR) Spectrometer, with flexible external optical configurations and various external detectors was used. First, direct transmission measurements were conducted with an external liquid nitrogen-cooled HgCdTe (MCT) detector. The FTIR's broadband beam was focused onto the metal side of the samples with a 250mm focal length Zinc Selenide (ZnSe) lens. The use of such a long focal length lens was important as it served to minimize the range of photon k-vectors impinging on the sample. Nonetheless, the focusing of the beam resulted in a variation of incident photon angle of  $\pm 5.5^\circ$ , which contributed to a broadening of the collected spectral features of the plasmonic structures studied. The transmitted signal was then collected and refocused onto the detector with a pair of 75mm ZnSe lenses. The direct transmission experiments are the coarsest measure of the sample quality, offering information on total transmission intensity and the spectral location of the peak.

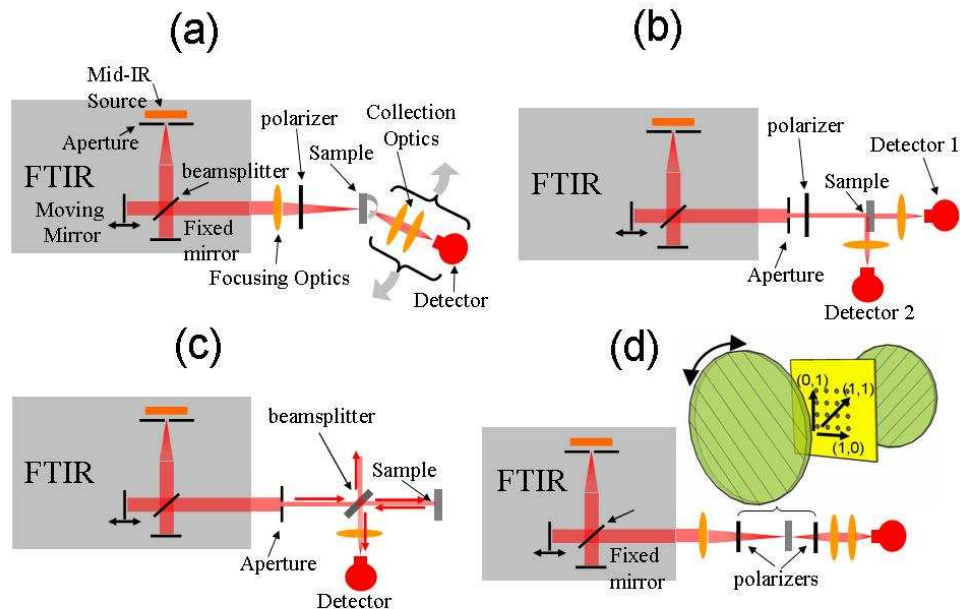


Fig. 1. Experimental set-ups utilized for full spectral and spatial analysis of EOT grating structures. (a) Coaxial independent rotation of sample and detector, allowing for experiments measuring normal transmission as a function of incidence angle and diffraction of normally incident light as a function of detector position. (b) Dual detection experiment for simultaneous measurement of transmitted and diffracted light. (c) Normal incidence reflection experiment. (d) Crossed polarizer experiment, with inset showing polarizer and sample orientations.

The direct transmission measurements, however, do not differentiate between non-transmitted light absorbed, reflected, or diffracted from the sample surface. While losses in EOT structures as a result of coupling to diffracted modes has sometimes been suggested as a significant loss mechanism [23, 24] very few works attempt to measure such losses when characterizing EOT structures. We constructed a custom-made co-axial rotational detection system as shown in Fig. 1(a), similar to that used in [25]. Both the sample and detector are mounted on coaxial automated rotation stages which allow for  $360^\circ$  rotation of the sample,

and approximately 200° rotation of the detector and signal collecting optics. This experimental setup allows for transmission measurements as a function of the angle of the incident light, as well as transmission/diffraction measurements as a function of the detector position. The latter set-up allowed for spectral measurements to be made over detector angles ranging from direct transmission (0°) to approximately 45 degrees off of normal reflection (135°). The angular dependent transmission and diffraction experiment allows for the study of light, which while neither reflected or absorbed by the sample, is lost to standard grating modes, or enhanced grating modes such as the Wood's Anomaly [26]

Following the angular detection experiment, we utilize a dual-detection scheme, Fig. 1(b), to focus on diffracted peaks identified at off-normal detector angles. In this experiment, the FTIR simultaneously collects spectra from both the normally transmitted light, and light at strong diffraction angles. By collecting two-channel spectral data, the relative strength of the EOT peak and the diffracted mode (in our experiment, the Wood's Anomaly) can be compared without alteration of the experimental optics.

In addition, normal incidence reflection data was collected from each of the 6 samples. In this experiment, depicted in Fig. 1(c), collimated light exiting the FTIR passes through a beam splitter, and reflects off of the sample surface. The light then reflects from the beam splitter to the collection optics. The sample reflection spectrum is then compared to reflection from a flat gold surface for reference purposes.

Lastly, a crossed polarizer experiment [27] was conducted using the experimental set-up shown in Fig. 1(d). The FTIR's broadband beam is focused with a 250mm focal length ZnSe lens through a wire grid polarizer which aligns the Electric field of the beam in the (1,1) grating direction (+45°). After transmission, the EOT spectrum is passed through a second wire grid polarizer oriented orthogonal to the first (-45°). Without the sample in place, no transmission is seen through the orthogonal polarizers. With a sample in place, incident light can couple to the ( $\pm 1, 0$ ), (0,  $\pm 1$ ), and ( $\pm 1, \pm 1$ ) SP modes. The second polarizer, however, will block any light whose transmission is not polarized in the ( $\pm 1, 0$ ) and (0,  $\pm 1$ ) directions, effectively isolating the polarization-dependent contribution to the EOT phenomenon. In the cross-polarizer experiment, the cross-polarizer (XP) transmission data is compared to parallel polarizer (PP) transmission data, where the two polarizers are both positioned at +45°.

The sum of these experiments allows for a rigorous analysis of transmitted, diffracted and reflected light. However, because we wish to understand the fate of all light incident upon an EOT grating near the primary resonance, we must also consider the effects of absorption. This is difficult, as the spectroscopic techniques employed in this work can only give a quantitative signal strength for the directly transmitted light. For the diffracted light, our set-up can only give a qualitative signal strength, as our detector only rotates around the "y" axis, and diffracted light should be observed for detector rotation around both the "y" and "x" axes. However, by measuring and comparing the diffraction, reflection and transmission spectra from our samples near the primary EOT spectral peak, we can qualitatively characterize the losses associated with each of these three phenomena, allowing for a better understanding of the geometry-dependent losses in these samples. By comparing the different epi-grown samples, into which we have engineered loss by the growth of doped epilayers, we can determine the material-dependent losses in our samples. The combination of the material- and geometry-dependent losses allows for a fuller understanding of the total losses in EOT structures.

### 3. Results

For each experiment, we will show a characteristic transmission, reflection or diffraction spectrum and when appropriate, compare this spectrum to the direct transmission spectrum of the same sample. We use, for our characteristic spectrum of each experiment, the 1 $\mu$ m undoped GaAs epilayer. If a significant variation in the spectral features as a function of doping density or thickness is seen for any experiment, we will show spectrum from the appropriate, more heavily doped material. However, for most experiments, the spectral

lineshapes do not vary significantly between samples, and it is sufficient to simply show the peak position of each phenomenon as a function of doping thickness and density.

Direct transmission through an EOT grating, as seen in Fig. 2(a), shows the well-characterized Fano lineshape [28] for the primary transmitted peak, corresponding to the  $(\pm 1, 0)$  SP modes. The inset of Fig. 2(a) shows the splitting of these degenerate modes as a function of sample angle, resulting from the non-zero in-plane momentum of the off-normal incident photons. Such transmission vs. sample angle plots can be used to generate the dispersion relation for surface modes on EOT gratings [29].

While the direct transmission experiments provide information on loss and tuning mechanisms in EOT gratings due to the dielectric of the semiconductor substrate upon which the gratings are deposited (by simple comparison of the peak transmission of the various samples studied), additional loss mechanisms can be identified by studying the light diffracted from the EOT structure. For instance, it has been suggested that the asymmetrical Fano lineshape of the EOT transmission spectrum could be a result of the spectral proximity of the Wood's Anomaly [23], the phenomenon in which the longest wavelength diffracted mode on a grating structure is enhanced [26]. If, in fact, the Wood's Anomaly affected the EOT process, it would be expected that this would be more pronounced in the mid-IR, where the large dielectric constants of metal increase the spectral proximity of the WA and EOT peaks. By rotating the detector and detector optics around the EOT grating sample, we are able to generate a plot of transmitted/diffracted light intensity as a function of wavenumber and of detector angle. The results for this experiment are shown in Fig. 2(b). Here we see the transmission of the  $(1, 0)$  and  $(1, 1)$  modes at detector angles close to  $0^\circ$  (direct transmission through the sample). As the detector rotates around the sample, diffracted light from the metal/air interface can be seen, as well as a strong diffracted peak at  $90^\circ$ , orthogonal to the incident light beam. This peak is the only identifiable diffracted beam from the semiconductor/metal interface, and is attributed to the Wood's Anomaly.

For this reason, our dual detector experiment was designed to simultaneously measure both the directly transmitted light, and that diffracted into the Wood's Anomaly. The Wood's Anomaly is a surprisingly strong signal, considering that the size of our grating structures (7mm x 7mm) requires this diffracted mode to travel through the semiconductor, near the metal/semiconductor interface for at least 3mm. In addition, though the Wood's Anomaly spatial signal in Fig. 2 is rather broad ( $85^\circ$  -  $95^\circ$ ), this is a result of the 1" collection optics used in the detector rotation experiment. A more accurate spatial measurement of this diffracted

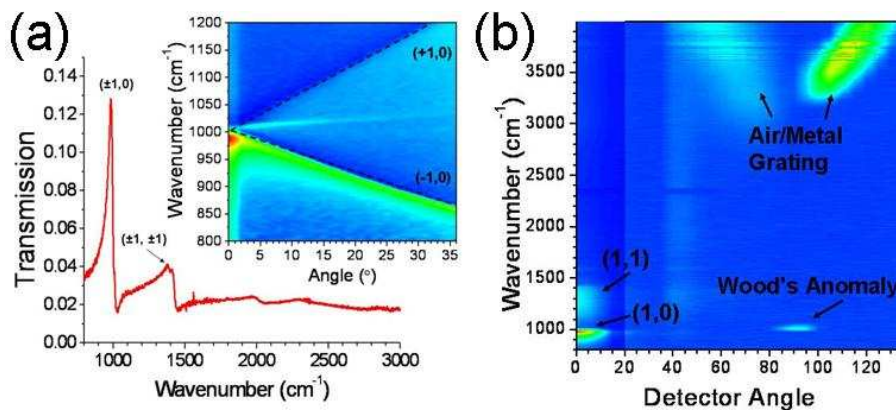


Fig. 2. (a) Spectrum of normally incident light directly transmitted through an EOT grating structure. The  $(\pm 1, 0)$  and  $(\pm 1, \pm 1)$  transmission peaks are labeled. Inset shows the transmitted light spectrum as a function of sample angle, demonstrating a clear splitting of the degeneracy of the  $(1, 0)$  and  $(-1, 0)$  transmitted peaks. (b) Surface contour plot of transmitted/diffracted light intensity as a function of wavenumber and detector angle. Identifiable are the directly transmitted  $(1, 0)$  and  $(1, 1)$  EOT peaks, the air/metal diffracted modes, and the Wood's Anomaly. Data from  $20$ - $135^\circ$  is scaled (x4) for ease of viewing.

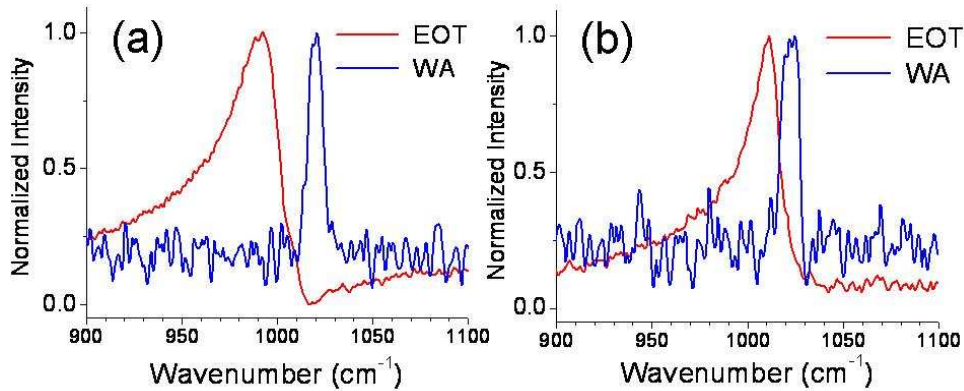


Fig. 3. Comparison of the EOT direct transmission and Wood's Anomaly diffraction spectra for (a) 1 $\mu\text{m}$  undoped GaAs and (b) 500 nm, doped  $10^{18}\text{cm}^{-3}$ , GaAs. Note the blueshift and lineshape change of the EOT peak at higher carrier concentrations.

light (using a translating slit to spatially map the WA mode) confirms that the Wood's Anomaly mode is actually spatially quite narrow, and tied closely to the metal/semiconductor interface.

The spectral comparison of the direct EOT transmission and the diffracted Wood's Anomaly, shown in Fig. 3, for all but the most heavily doped sample, show the diffracted peak to coincide almost exactly with the EOT transmission minima on the high energy side of the (1,0) peak. In the most highly doped sample (500nm,  $1\text{E}18\text{cm}^{-3}$ ), the increase in the semiconductor doping leads to a significant shift in the peak position of the (1,0) EOT mode, and the Wood's Anomaly, whose spectral position does not shift appreciably, now sits on the falling edge of the EOT transmission. For all of the samples studied, the intensity of the WA peak is weaker, but within an order of magnitude of the direct EOT peak intensity. A more quantitative measurement of the WA strength is difficult, as the detected WA signal could be affected by sample processing defects far from the EOT grating (chipped sample edges, for instance), total sample size (the border of the EOT grating), or the position of the incident light on the grating surface, all of which would have no effect on the direct EOT signal, but could degrade the WA signal.

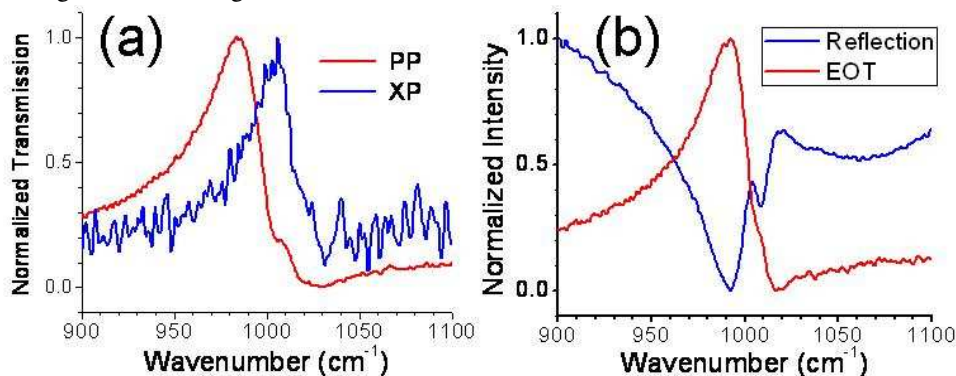


Fig. 4. (a) Comparison of the normalized Parallel and Crossed polarizer (PP, XP) transmission spectra. While the PP spectrum shows the same lineshape and peak position as the EOT spectrum for this sample, the XP spectrum is blue-shifted, sitting on the high energy falling edge of the PP spectrum. Furthermore, the XP spectrum does not have a Fano lineshape, but instead appears closer to a Lorentzian peak shape. While the plots are normalized, the weak signal to noise ratio of the XP spectrum is indicative of the weaker signal associated with this transmission. (b) Comparison of the normalized EOT and reflection spectra. The reflection data shows two significant dips, the first at the peak EOT spectral position, the second to the high energy falling edge of the primary EOT peak.

In the cross-polarizer (XP) experimental set-up, the nonresonant transmission through the grating is suppressed, while the transmitted light corresponds to polarization dependent excitations in the EOT structure [27]. The XP transmitted light gives extremely weak and noisy signals, even with significant averaging of the collected spectra. The ratio of the PP to XP peak signal intensity is on the order of 15-25, depending on the sample studied, and for the most highly doped sample, no XP signal was detectable. In addition, the spectral peaks of the XP and PP transmission spectra are not coincident. The XP spectra, for every sample studied, lies on the high energy falling edge of the PP transmission data. A representative XP transmission spectrum is shown in Fig. 4(a).

Finally, normal incidence reflection data was collected for each sample. The reflection spectra consistently show two minima in the reflected light. The first and strongest minima corresponds to the transmission of the primary EOT mode, while the second sits, like the XP transmission spectra peaks, on the high energy falling edge of the EOT peak. A representative reflection spectrum is shown in Fig. 4(b).

#### 4. Discussion

A clearer picture of the competing transmission, reflection, and diffraction phenomena on EOT gratings can be obtained by plotting all of the spectra simultaneously, as shown in Fig. 5. The EOT, the Wood's Anomaly diffraction, and the XP transmission all peak at independent spectral positions. By comparing the spectra in Fig. 5, we can not only determine the relative spectral position of each phenomenon investigated, but we are also able make a qualitative assessment of the strength of the coupling to, and loss associated with, each mode by comparing the collected light for the phenomenon of interest to the reflected light at that same wavelength. The relationship between fractional absorption (A), diffraction (D), transmission (T) and reflection (R),  $R=1-(A+D+T)$ , allows us to extract a relative absorption strength as a function of wavelength. The reflection experiment shows two strong spectral dips, one at the direct EOT wavelength, and the other at the wavelength of the XP transmission peak. At these two wavelengths, the light that is not reflected must either be transmitted/diffracted or absorbed. If the diffracted or transmitted intensity is weak at these wavelengths, it suggests that significant light is absorbed by the sample. Thus, a strong dip in reflection, combined with a weakly transmitted/diffracted signal (as is seen at the wavelength of the XP transmission peak), indicates strong coupling to a high loss mode, since the light incident upon the sample at this wavelength is not collected with a significant intensity in any of our experimental configurations. However, the absence of a reflection signature, combined with a relatively strong transmitted/diffracted signal (as is the case at the wavelength of the WA peak), suggests weak coupling (since most of the light is reflected), but low loss (as the WA signal is quite distinct). The qualitative determination of the coupling strength and losses of each phenomenon are presented in the table included in Fig. 5.

Because we are able to spatially and spectrally collect a large portion of the radiation interacting with the EOT grating, a complete picture of the grating-related losses can be determined. However, in order to develop semiconductor-based plasmonic structures, material losses must also be characterized. Fig. 6 shows the peak transmission intensity as a function of both doping density (for a fixed, 250 nm thick doped layer) and doping thickness (for varying epilayer thicknesses, each doped  $1E18\text{cm}^{-3}$ ). Both plots show a distinct decrease in intensity as a function of increased doping.

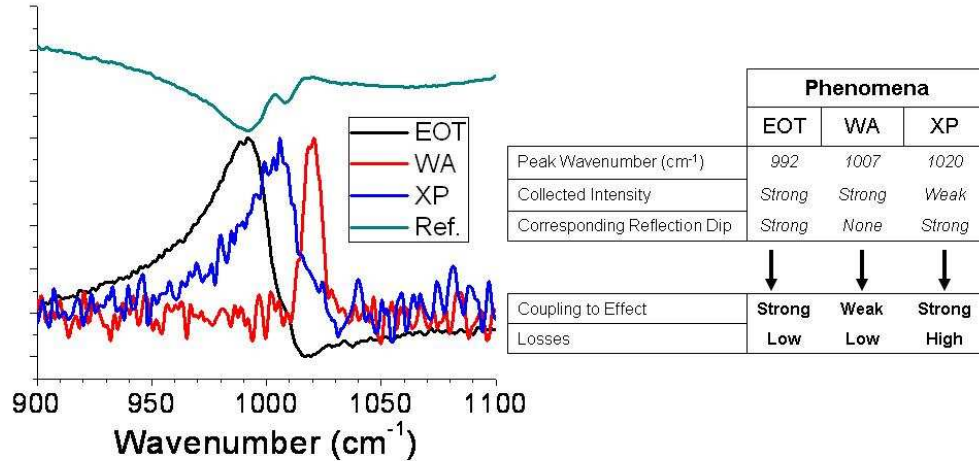


Fig. 5. Comparison of normalized EOT, WA, XP, and reflection (Ref.) spectra for sample A. The reflection data has been vertically offset for clarity. The table (right) shows the relative strength of the collected signal for each phenomenon (EOT, WA, and XP), compared to the strength of the dip in the reflection spectrum at the peak wavelength of each effect (EOT, WA, and XP). At the wavelength of the EOT peak, a strong dip in reflection is seen, suggesting strong coupling, and low losses. The distinct WA peak has no corresponding reflection dip, suggesting weak coupling, and low losses. Finally, the weak XP signal peak corresponds to a noticeable reflection dip, indicating strong coupling, but high losses.

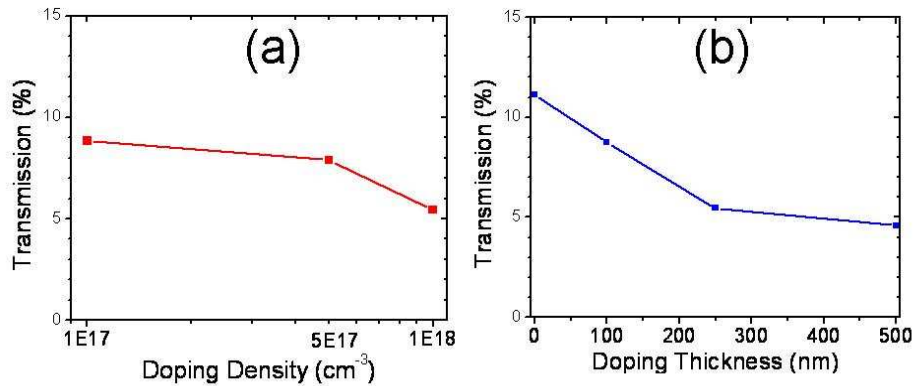


Fig. 6. Transmission through EOT grating structure as a function of (a) Doping concentration, for a doped epilayer of fixed width (250nm) and (b) Doped epilayer thickness, for a fixed doping concentration of  $1\text{E}18\text{cm}^{-3}$ .

In addition, we can track the peak position of the spectrum for each effect as a function of doping thickness and carrier density. Clear shifts are seen in the peak position for the EOT, XP, and Reflection spectra, but relatively little shift is seen for the Wood's Anomaly peak. The doping layers, even at their thickest, are still well within one wavelength of the surface. This strongly suggests that the EOT and XP phenomenon are tightly bound to the metal/semiconductor interface, as changes of doping, even within 100nm of the interface, can induce strong peak shifts in these spectra. The Wood's Anomaly, however, would appear to

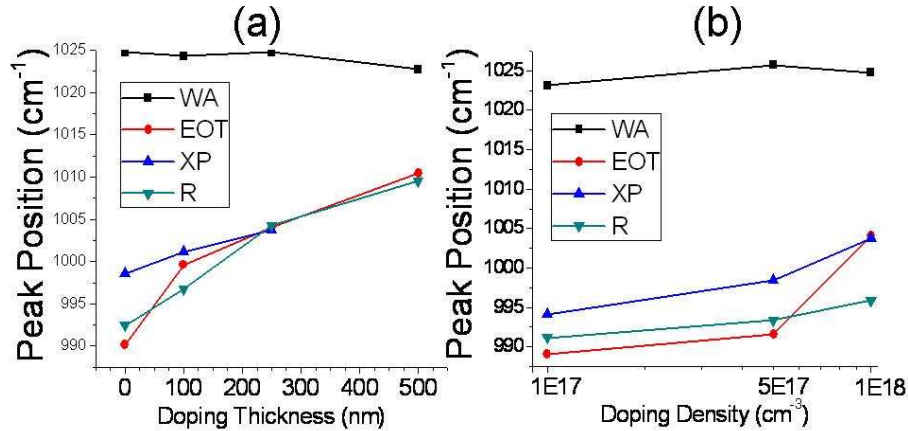


Fig. 7. Peak positions for EOT, WA, XP, and Reflection data as a function of (a) Doping thickness and (b) Doping density. While the EOT, XP, and Reflection data each show significant shifts with doping, as the dielectric constant of the semiconductor is tuned at the metal/semiconductor interface, no such tuning of the Wood's Anomaly is observed.

be more loosely bound, as doping near the interface does not strongly affect the WA peak position. This result is reinforced by the strength of the WA signal, which, in the mid-IR, would be strongly attenuated by free carrier losses, were it closely bound to the surface, and traveling through many millimeters of highly doped material. Because the WA mode is determined to be low-loss, the WA itself could not be tightly bound to the metal surface.

## 5. Conclusions

In summary, the spatial and spectral transmission, diffraction, and reflection of EOT gratings with engineered material losses have been measured. In addition, the effects of Wood's Anomaly and the polarization dependent surface plasmon coupled portion of the EOT effect have been isolated, measured, and compared. These experiments, on the one hand, allow us to effectively track every photon incident on the EOT grating near the primary EOT peak. We are able to qualitatively label the various modes as either high or low loss, and measure the relative coupling strength to each mode. Moreover, by engineering losses in the dielectric substrate upon which the EOT grating is deposited, we can better understand the material losses associated with the gratings, and determine whether each phenomenon studied is tightly or loosely bound to the metal/dielectric interface. Finally, by limiting the total number of excess charge carriers employed for permittivity tuning, strong transmission with effective peak shifting can be achieved for use in actively tunable EOT devices.

## Acknowledgments

This work was supported in part by the U.S. Air Force Research Lab under contract FA8650-08-C-1445. Sandia is a multiprogram laboratory operated by Sandia Corporation, a Lockheed Martin Company, for the United States Department of Energy's National Nuclear Security Administration under contract DE-AC04-94AL85000.